Buckling-Based Strong Dry Adhesives Via Interlocking

*Chi-Mon Chen, Chang-Lung Chiang, Chien-Lin Lai, Tao Xie, and Shu Yang**

High-aspect-ratio shape-memory polymer (SMP) pillar arrays are investigated as a new type of dry adhesive based on buckling and interlocking mechanism. When two identical SMP pillar arrays are engaged at 80 °C, above the glass transition temperature at a preload larger than the critical buckling threshold, the pillars are deformed and become interweaved and/or indented with each other. After cooling to room temperature, strong pull-off forces are observed in the normal and shear directions, both of which are much larger than those from pillar-to-flat surface and flat-to-flat surface contact. From finite element anaylsis (FEA) and comparison of measured and calculated adhesion values using different contact mechanics models, it is shown that interweaved pillars are the main source that contributes to the pillar-to-pillar adhesion and the indented pillars set the lower limit, whereas the probability of interdigitation is very low. Further, it is found that interweaved pillars are primarily responsible for the decreased adhesion strength and increased anisotropy when the pillar spacing became larger. Finally, it is shown that the bonded pillars can be easily separated after reheating to 80 °C due to significant drop of modulus of SMPs.

1. Introduction

Adhesion between polymers plays an important role in a wide range of industrial applications, including electronic packaging and automotive and airplane assemblies. Compared to liquid based adhesives, dry adhesives as manifested in gecko foot hairs are attractive because they require no liquid handling or lengthy curing during the adhesive attachment and the adhesion strength can be rapidly switched. The ability of gecko to cling on almost any surface is attributed to the split contact adhesion resulting from millions of hierarchical fibrillar structures on its toe pads via the weak non-covalent van der Waals force and/or capillary forces.[1–3] Specifically, it has been shown that the directional tilt of the fibrillars and a lateral friction force play the critical role in the gecko's articulation of attachment and detachment.[4–6] High net friction and adhesion forces are obtained at small pulling angles between the spatulae and the substrate. For detachment, the spatulae are peeled off perpendicularly from the substrate, leading to reduction of adhesion and friction force over three orders of magnitude. There have been numerous attempts to fabricate synthetic gecko-like adhesives with fibrillar architectures of variable size, shape and tip geometry as well as different degree of tilting of the fibrillar structures.[7–20]

In comparison, dry adhesives based on collective mechanical interlocking forces, such as those exhibited in the Burdock seeds with many small hooks and loops, have received relatively less attention until recently. The discovery of the interlocking mechanism in Burdock seeds led to the invention of Velcro tape,[21,22] which could have a very large adhesion strength (≈120 N/cm^2)[23] to hold a person and automotive body parts using the Velcro tape. This is because any force pulling the hooks/loops apart is spread evenly across all hooks and the strength of the bond depends on how well the hooks are embedded in the loops. Different from gecko adhesion, when a force is applied in the normal direction or pulled in a direction parallel to the plane of the Velcro surface, more hooks and loops are engaged, thus, adhesion strength increases.

Insects such as beetle and dragonfly employ similar type of interlocking adhesion mechanisms.[24] Many beetles have arrays of protrusions on their elytra and wings. These features attach the elytron to the wing when the beetle is at rest, offering the resistance to be sheared and preserving the easiness of spanning the wings.[25,26] A certain species of dragonflies has tapered cuticles on the head and the neck to lock the head in place by friction during feeding or tandem flight.[25,27]

Recently, several groups have begun to investigate adhesion between two structured surfaces, including identical random nanowires,[28,29] periodic arrays of high-aspect-ratio polymers pillars,[26] and complementary ripples.[30,31] The interlocked nanowires and pillars show highly anisotropic adhesion, where the shear adhesion is much larger than the normal adhesion. This is because the engagement and alignment of nanowires/pillars in the shear motion promotes the contact area between them. In the case of periodic polymer pillar array imitating the beetle wing structures, the adhesion is anisotropic[26,32] and preload dependent.[33] The adhesion also increases monotonically with pillar aspect ratio.[26] In a separate vein, McMeeking and co-workers developed a theoretical model for a friction-based fastener, mimicking the dragonfly head arrester. Such fastener is expected to achieve an adhesion strength that is ≈30%

C.-M. Chen, C.-L. Chiang, C.-L. Lai, Prof. S. Yang
Department of Materials Science and Engineering
University of Pennsylvania
3231 Walnut Street, Philadelphia, PA 19104, USA
E-mail: shuyang@seas.upenn.edu
Dr. T. Xie
Bio and Nanomaterials Technologies Department
Sensors and Materials Laboratory
HRL Laboratories
LLC, 3011 Malibu Canyon Road, Malibu, CA 90265, USA

DOI: 10.1002/adfm.201300052

of the tensile strength of the material.[27] However, in reality, engaging such adhesives would be difficult and could be further complicated by structural buckling.[27] So far, researchers have attempted to avoid buckling and collapse of the pillars in the adhesion study using well-ordered pillars as model systems since buckling and collapsing of the pillars will complicate the interpretation of the pillar-pillar contact, not to mention that it will be very difficult to image such interface.[26,27,34,35] However, instability exists commonly in bioorganisms, and practical samples. Therefore, it will be critically important to understand the impact of buckling of the pillars at the interface, specifically, to the interlocking adhesion strength.

Here, we demonstrated a strong dry adhesive through interlocking of two complimentary sets of buckled shape memory polymer (SMP) pillar arrays above the glass transition temperature (T_g, 60 °C) under a load. When engaged at 80 °C, the SMP pillars became rubbery; they interweaved and/or indented with each other at a preload larger than the critical buckling threshold. After cooling down to room temperature, the interlocked pillars were fixed in a glassy state. It required strong forces at room temperature to separate the two pillar surfaces, ≈53.6 ± 25.1 N/cm^2 in the normal direction and ≈71.9 ± 23.2 N/cm^2 in the shear direction for cylindrical pillars in a hexagonal lattice (1 μm diameter, spacing 1 μm, and aspect ratio 4). Both adhesion values were much larger than the corresponding adhesion from a pillar-to-flat surface contact (12.3 ± 8.8 N/cm^2, normal, and 15.0 ± 2.3 N/cm^2, shear) and a flat-to-flat surface contact (7.1 ± 5.0 N/cm^2, normal, and 15.8 ± 2.0 N/cm^2, shear). Despite the strong adhesion exhibited by the interlocked pillars, the two pillared surfaces could be easily separated by reheating to 80 °C through the release of the elastic energy stored in the deformed (i.e., buckled) state. Further, we showed that the adhesion could be tuned by varying the pillar spacing. By comparing the experimental results with theoretical calculation and finite element simulation, we elucidated the buckling based interlocking adhesion mechanisms.

2. Results and Discussion

It is known that adhesion between materials is mediated by their surface or near-surface properties, including 1) local chemistry to affect intrinsic adhesion at the molecular level, 2) microscopic surface roughness (topography), 3) macroscopic materials mechanical properties (compliance), and 4) the effective contact, which is dependent on the magnitude and type of the loading applied to the surface. In the past decade many gecko-inspired dry adhesives have been fabricated, which almost exclusively exploit the surface geometric effect for adhesion enhancement. Few have explored manipulation of materials intrinsic properties, including local chemistry at the molecular level,[36,37] and tunable bulk modulus.[12,38,39] It has been shown that interlocking between identical or complementary structured surfaces could offer strong and anisotropic adhesion.[26,28,29,40] However, detailed insights of the interfacial interaction between two sets of microstructured surfaces, its dependence of geometry and bulk modulus, and the resulting macroscopic adhesive properties remain lacking in the literature.

SMPs are materials that can memorize temporary shapes and recover to their permanent shape upon exposure to an external stimulus, such as heat, light, and solvent.[41–43] The "permanent" shape is typically achieved by chemical or physical crosslinking. Above a thermal phase transition temperature, either a T_g or a melting transition temperature (T_m), the polymers can be deformed. Upon cooling, the deformed "temporary" shape can be fixed. Near the phase transition temperature, an SMP changes from the glassy state to the rubbery state with 2–3 orders of magnitude change of the elastic modulus. The low modulus at the rubbery state facilitates intimate interfacial contact between two opposing surfaces for bonding, whereas the high modulus at the glassy state favors high adhesion in the bonded state. The entropic energy stored in the deformed state can be later released on demand in the shape recovery process to trigger automatic debonding. Recently, SMPs have been used in micropillars (≈10 μm in diameter) to thermally control gecko-like dry adhesion, that is, contact between pillar and flat surface, by coating a thin adhesive layer on the tips of SMP micropillars[39] or directly patterning SMP pillars.[12] Both studies showed that temperature played a key role to tune the bulk materials stiffness and the effective contact through deformation or tilting of the pillars.

We are interested in interlocking adhesion through pillar-pillar contact and tuning the effective modulus of the SMP pillars at different temperatures for controlled bonding and debonding, specifically, how buckling of the pillars could impact their interfacial interactions. Utilizing replica molding (**Figure 1**), we fabricated cylindrical SMP micropillars in a hexagonal lattice with pillar diameter of 1 μm and aspect ratio (AR = height/diameter, h/d) of 4. The pillar-to-pillar spacing was varied as 1 μm and 2 μm. Here, the SMP was epoxy based from diglycidyl ether of bisphenol A epoxy monomer (BADGE), poly(propylene glycol) bis(2-aminopropyl ether) (Jeffamine D-230) and decylamine (DA) (see **Figure 2**). The BADGE, Jeffamine D-230 and DA were mixed in a molar ratio of 4:1:2 to obtain an SMP with T_g of 60 °C. Dynamic mechanical analysis (DMA) showed that the storage modulus dropped approximately 3 orders of magnitude, from 2.5 GPa at 22 °C (glassy state) to 3.6 MPa at 80 °C (rubbery state, Figure 2b). Likewise, the tensile modulus was found to drop from 2.2 GPa at 22 °C to 3.1MPa at 80 °C.

Two sets of identical pillars were pressed against each other at 80 °C under a preload. Under this condition, the pillars were softened and deformed. While maintaining the load, the pillars were cooled down to room temperature to fix the deformed states of the pillars (see **Figure 3**a). This completed the bonding process. The adhesion forces were measured in the normal and shear directions at both 80 °C and room temperature to study temperature dependent detachment (see the setup for macroscopic adhesion measurement in Supporting Information Figure S1). The results were compared to those from pillar-to-flat and flat-to-flat samples to evaluate the enhancement of dry adhesion strength and anisotropy by the interlocking mechanism.

There are three possible scenarios of pillar-to-pillar contact: 1) interdigitation, 2) indenting, and 3) interweaving (Figure 3b–d). When the preload is small, the pillars remain

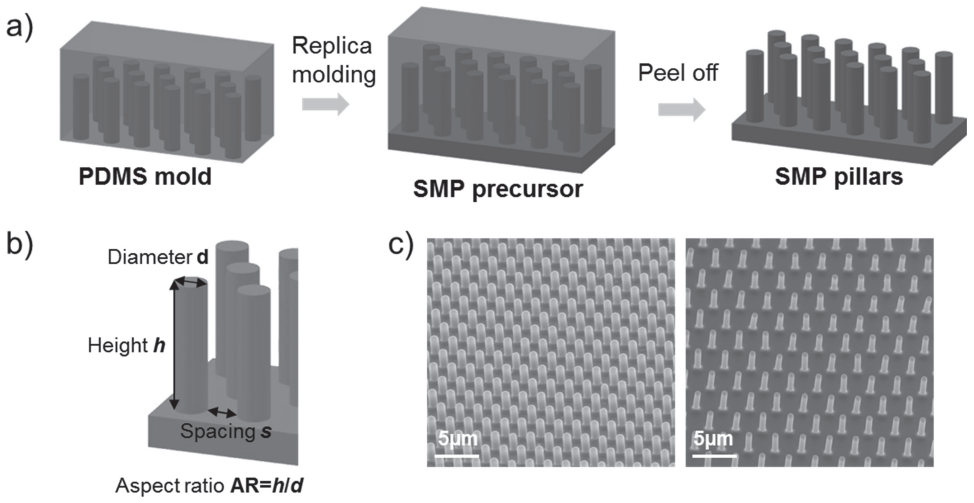

Figure 1. Fabrication of shape memory polymer pillars via replica molding. a) Schematics of the fabrication process. b) Characteristics of pillars. c) SEM images of SMP pillar arrays in a hexagonal lattice with $d = 1$ μm, $s = 1$ μm (left) and 2 μm (right), and AR = $h/d = 4$.

straight and can interdigitate with pillars from the other set of sample (Figure 3b). In this case, the adhesion could be amplified by increasing the effective contact area as demonstrated by Suh and co-workers.[26] The possibility of interdigitation, however, as we show below is limited by pillar geometry. Here, a spacing parameter α is introduced as:

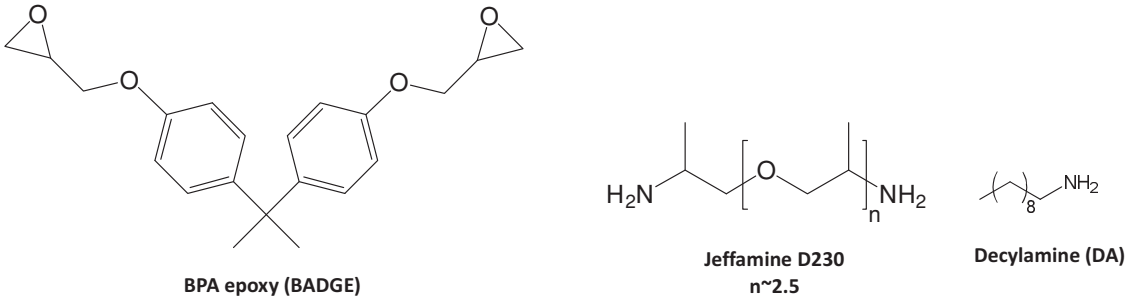

(a)

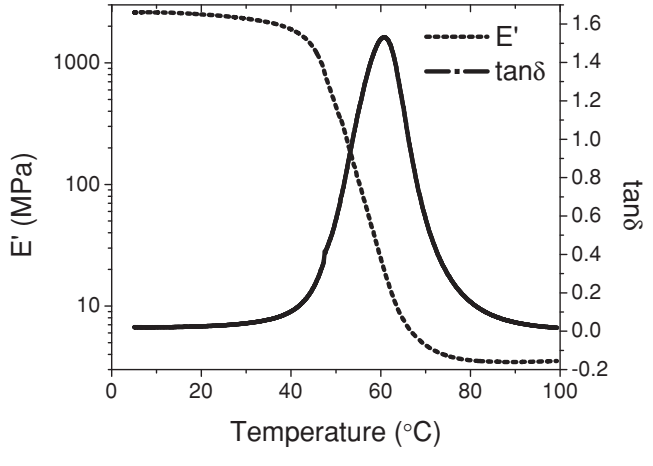

(b)

Figure 2. Shape memory polymer composition and thermomechanical properties. a) Chemical structures of the ingredients. b) Storage modulus (E') and loss tangent (tanδ) as a function of temperature measured by dynamic mechanical analysis. T_g is ≈60 °C from the mixture of bisphenol A diglycidyl ether, Jeffamine D-230 and decylamine in a molar ratio of 4:1:2.

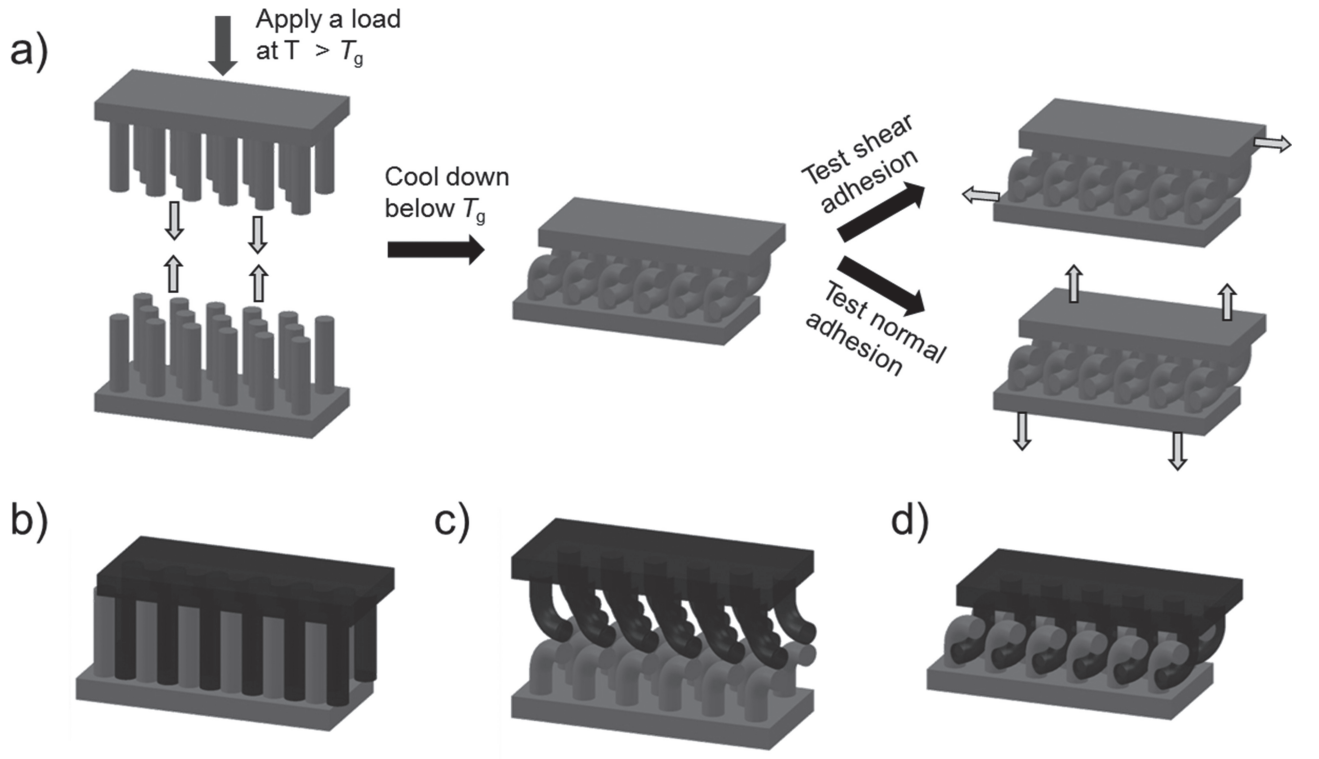

Figure 3. a) Illustration of engaging pillar-to-pillar contact and adhesion measurement. b–d) Three possible interlocking modes between two sets of identical SMP pillar arrays: b) interdigitation, c) indenting, and d) interweaving.

$$\alpha = 1 + \frac{s}{d} \tag{1}$$

where d is the pillar diameter and s is the spacing between pillars (see definition in Figure 1c).

Considering two pillar arrays to interact with each other with only translational degree of freedom (no relative rotation), the probability of interdigitation, $P_{i,}$ for a hexagonal lattice is dependent solely on α,

$$P_i = \left(1 - \frac{2\pi}{\sqrt{3}\alpha^2}\right) - \frac{3}{\alpha^2}\cos^{-1}\left(\frac{\alpha}{2}\right) - \frac{3}{2\alpha}\sin\left[\cos^{-1}\left(\frac{\alpha}{2}\right)\right] \tag{2}$$

for $2 > \alpha \geq \sqrt{3}$, and

$$P_i = 1 - \frac{2\pi}{\sqrt{3}\alpha^2} \tag{3}$$

for $\alpha \geq 2$.

For $\alpha < \sqrt{3}$, the interdigitation does not occur. In our system, for $\alpha = 2$ ($s = 1$ μm) and $\alpha = 3$ ($s = 2$ μm), $P_i = 9.31\%$ and 59.69%, respectively (Supporting Information, Figure S2a). These values explain why the interdigitation can be achieved in the system reported by Pang et al., which has $\alpha = 3$.[26] For pillars with $\alpha = 2$ in our system, the geometrical interdigitaion is highly unlikely, especially when the relative rotation is involved, which is difficult to avoid experimentally (Supporting Information, Figure S2b).

In the other extreme, as $\alpha \approx \sqrt{3}$, McMeeking et al.[27] showed that it was possible to have a strong frictional adhesion comparable to the tensile strength of the material. It is, however, very difficult to engage the pillar in the first place, which is further complicated by the elastic buckling of the pillars. For a circular pillar, the critical buckling stress σ_{cr} can be calculated by fixing one end of the pillar to the substrate and pinning the tip as the boundary conditions by assuming the frictional force generated due to contact with the substrate, which restricts the horizontal displacement of the pillar tip,[44,45]

$$\sigma_{cr} = \frac{20.19E}{16AR^2} \tag{4a}$$

where E is the elastic modulus of the pillar. On the other hand, if the two pillar tips are considered as free ends, the critical buckling stress then becomes,[45]

$$\sigma_{cr} = \frac{\pi^2 E}{64AR^2} \tag{4b}$$

First, the two sets of pillars were brought into contact at 80 °C in the rubbery state at an apparent preload of 24 N/cm^2. When normalized by the pillar areal density, the effective preload became 1.06 MPa for $\alpha = 2$ and 2.38 MPa for $\alpha = 3$ pillars, well above the buckling threshold (σ_{cr} = 0.25 MPa from Equation 4a or 0.03 MPa from Equation 4b). Therefore, the softened pillars would be bent and collapsed against each other at 80 °C, leading to indentation (see Figure 3c) and/or interweaving much like weaved yarns (see Figure 3d). As seen in **Figure 4**, both modes of pillar-to-pillar contact were experimentally observed. It is intriguing how the pillar-to-pillar interactions will affect the effective adhesion force and anisotropy in comparison to the pillar-to-flat and flat-flat configurations, and whether it is possible to detach them on demand.

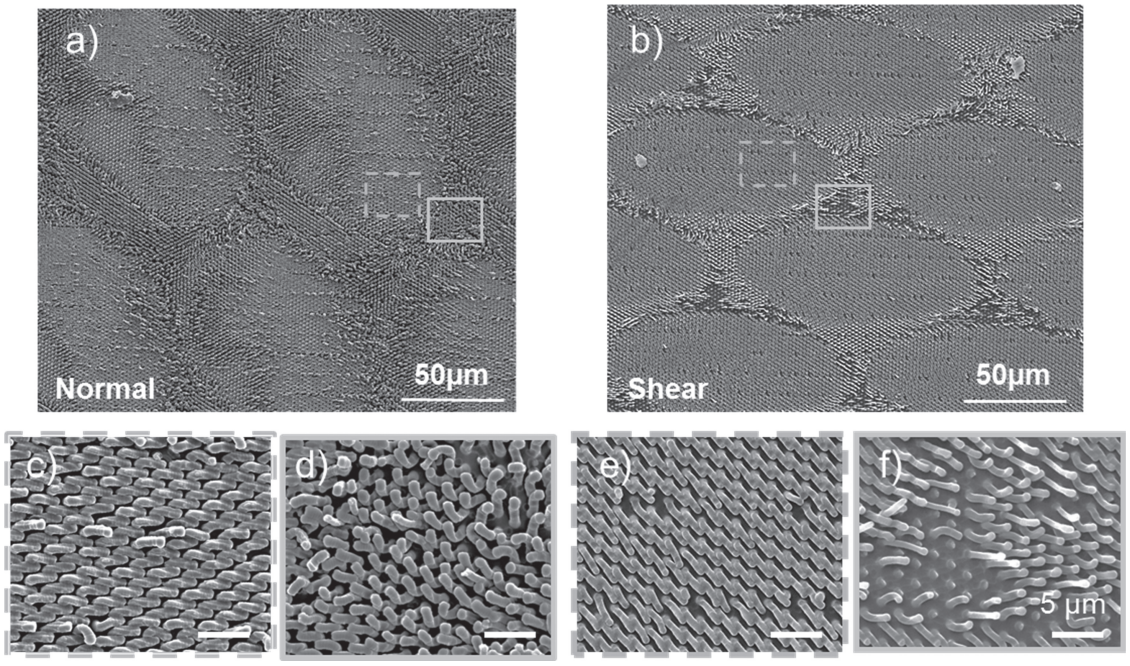

Figure 4. SEM images of indented and interweaved pillars after being engaged at 80 °C and subsequently separated at room temperature in the normal separation direction (a) and shear separation direction (b). c–f) Corresponding higher magnified areas: c,e) indented pillars and d,f) interweaved pillars. In panels (c–f) the scale bars are 5 μm.

Moiré patterns, which are commonly formed when two or more geometrically regular patterns are superimposed,[46] were observed after separating the interlocked pillar arrays (see Figure 4a,b). Recently Kang et al. also reported Moiré patterns when evaporating water sandwiched between two periodic pillar surface.[47] As seen in Supporting Information Figure S3, when the relative rotation angle between two compressed pillar array reaches 10°, Moiré pattern is formed with a characteristic period, which decreases as the rotation angle increases. A closer look of the Moiré pattern from 10°-rotation in Supporting Information Figure S3 suggests that there are different degrees of mismatch between pillar pairs depending on whether the pillar tips are in contact with the counter surface. Presumably, the predominant mode of interaction between two contacting pillars would be indenting as they buckle and deform together in response to the load. However, it is very difficult to directly image the pillar-to-pillar contact geometry at the interface at different contact stages as the pillars were interweaved or indented to each other. To better understand the contact process, we used Abaqus finite element analysis (FEA) to simulate the interaction between a pair of pillars, which were then compared to the SEM images of the separated pillars after engagement. The pillar pairs were slightly misaligned at the beginning near the tips, under a load at 80 °C (**Figure 5**). Above T_g, when the load was greater than the buckling threshold, the pillars were deformed and pushed against each other since the initial contact started at the tips. At the final stage of the deformation, the pillars became indented to each other. In contrast, when pillars were completely mismatched with each other at the beginning, the primary mode of pillar-to-pillar contact would be interweaving since the pillars would not buckle until they became interdigitated and sliding against each other while they might or might not reach the bottom surface of the

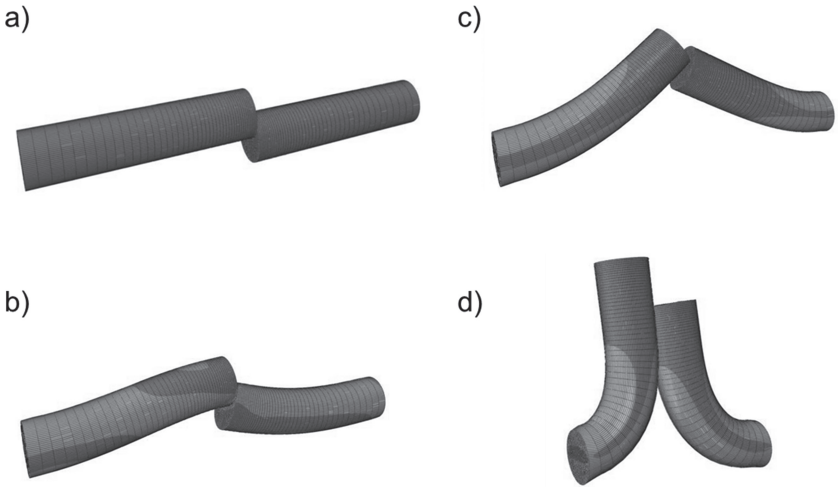

Figure 5. Finite element simulation of the contact process between a pair of pillars under load at 80 °C using Abaqus 6.10-1. The pillars pair is originally in a partially misaligned state (a). One side of the pillar is compressed and deformed toward the other pillar by apply a ramping displacement (b,c), and reaching the final state (d).

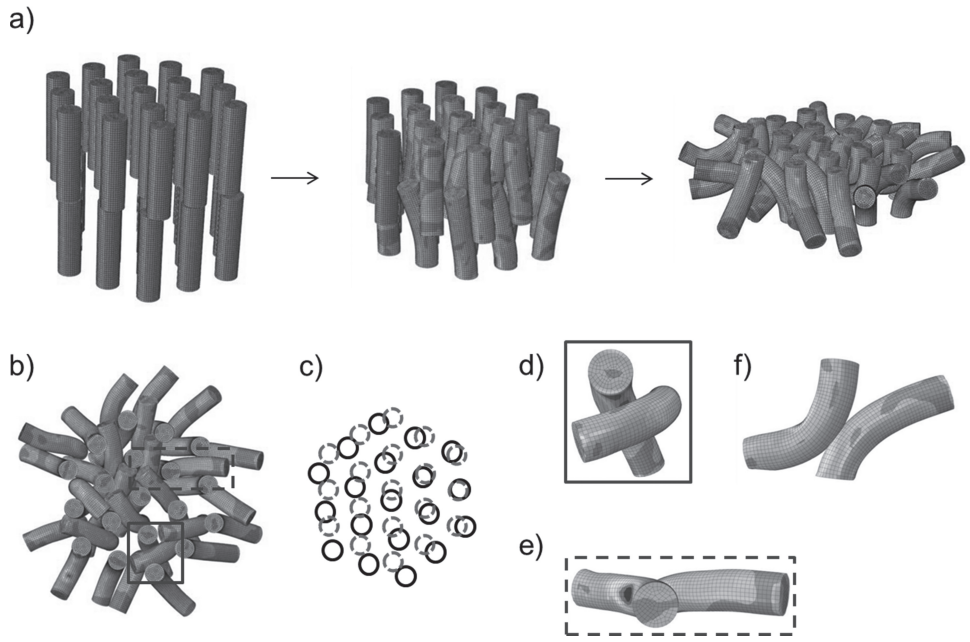

Figure 6. Finite element simulation of the contact process between two sets of pillars in a hexagonal array. a) The collapsing process of the compressed pillars. b) Bird's eye view of the fully compressed pillar arrays. c) The mapping of two sets of interacting pillar bases, showing the relative position of pillars. Solid circles represent the set of bases directly observable in (b). The dashed circles represent the set underneath. The interweaved (d) and indented (e) pillars. f) The side view of (e).

counter pillars. To capture the collective behavior of multiple pillars at the pillar-pillar interface, we then simulated the contact process of pillars in a hexagonal array (**Figure 6**) with the same degree of misalignment as the one seen in Figure 5 but with an additional rotation of 10°. This rotation is exaggerated comparing to the experimental condition where a relative rotation <3° is normally observed. This is chosen to account for the relative small pillar array in the simulation of multiple pillars vs. the real macroscopic sample. The interaction was found anti-symmetric at the beginning until reaching the point where multiple pillars were interacting with each other. The contact process is much more complex than that from a single pair. This is because when the symmetry of the pillar array is broken upon buckling, the pillars could slide and enter the open spaces available on the other set of the pillar array. Finally, when the pillars were totally collapsed, both interweaving (Figure 6d) and indenting (Figure 6e,f) pillars were observed in simulation, which agreed well with experimental results shown in Figure 4. Indented pillars were often observed in the region with more pillar-to-pillar contact (by comparison of SEM images with simulated Moiré pattern in Supporting Information Figure S2), whereas interweaved pillars appeared in the region with less pillar-to-pillar contact. This can be further visualized from the pillar base mapping of Figure 6c (see Figure 6d), where the pillar pairs with large fraction of overlapping base area primarily indent with each other. Interestingly, Figure 6c also suggested that the pillar pairs bent as a result of indenting can also interweave with other neighboring pillars. The highly angle-dependent morphology could potentially contribute to a relatively large deviation in the adhesion force measurement, which we will discuss in detail later.

After the preload at an elevated temperature, the interlocked samples were cooled down quickly to room temperature to lock the structure. Upon cooling, the elastic modulus increased dramatically back to 2.5 GPa (storage modulus) and 2.2 GPa (tensile modulus), respectively. The interlocked pillars will resist any deformation for separation and we should expect a large adhesion force. As a comparison, samples were also prepared under the same preload and temperature cycle by pressing a SMP pillar array against a flat SMP (pillar-to-flat) or pressing two flat SMP films (flat-to-flat) together. Indeed, as shown in **Figure 7**a,b, the pillar-to-pillar (α = 2) adhesion measured at room temperature was 53.6 ± 25.1 N/cm^2 in the normal direction and 71.9 ± 23.2 N/cm^2 in the shear direction. These adhesion values were significantly larger than those from either the pillar-to-flat (12.3 ± 8.8 N/cm^2, normal and 15.0 ± 2.3 N/cm^2, shear), or from the flat-to-flat samples (7.1 ± 5.0 N/cm^2, normal and 15.8 ± 2.0 N/cm^2, shear).

In the case of the interweaved pillars, the difference between the normal and shear adhesion would be dependent on the lever arm of bending. Using Castigliano's first theorem,[48] the normal force P required to separate a single pair of interweaved pillars is

$$P = \frac{\delta^P E I}{\left(\frac{L_2^3}{3} + \frac{\pi L_2^2 R}{2} + L_2^2 L_1 + 2 L_2 R^2 + 2 R L_1 L_2 + R^2 L_1 + \frac{\pi R^3}{4}\right)} \quad (5)$$

where δ^p is the deflection in the normal direction, I is the area moment of inertia, L_1, L_2 and R are the base length, arm length and the bent radius, respectively (Supporting Information Figure S4a). For shear force S to separate the interweaved pair of pillars, it is given by

$$S = \frac{3\delta^S E I}{L_1^3} \tag{6}$$

where δ^S is the deflection in the shear direction (Supporting Information Figure S4a).

Based on Equations 5 and 6 and assuming L_1 = 1 μm, L_2 = 1 μm, R = 1 μm and the deflections $\delta^p = \delta^S$ = 1.5 μm, we obtained P = 538 N/cm^2 and S = 9352 N/cm^2 after normalized by the area occupied by the pillars. Compared to the normalized ultimate tensile stress of the polymer (≈893 N/cm^2), it is expected that pillars should fracture easily in the shear test. Simulation (Supporting Information Figure S5) suggested that the stress could be concentrated at the pillar base, and more so in the shear force. Here, the interaction force was set as a point load equal to the averaged experimental adhesion force/area. In agreement with the simulation, experimentally we did find fractured pillars in the interweaved regions for both normal and shear force of separation, but more apparent in the later (see Figure 4d vs. f).

In the case of the indented pillars, the adhesion can be analyzed by contact mechanics models. Considering two extreme contacting scenarios between two cylinders, which are either in parallel (Supporting Information Figure S4b) or perpendicular (Supporting Information Figure S4c) configuration with each other under a normal pull-off force or sliding against each other under a shear force (Supporting Information Figure S4e). The adhesion between parallel-contacting cylinders can be formulated as:[49]

$$F = \left(\frac{\pi E W^3 d^2}{8(1-\upsilon^2)}\right)^{1/4} \left(\frac{L_c}{2}\right)^{3/4} \tag{7}$$

where L_c is the contact length, ≈3 μm, W is the work of adhesion, 38 mJ/m, ν is the Poisson's ratio, which equals to 0.45 for the SMP[50] (Supporting Information Figure S4b). After normalized by area, F = 18.3 N/cm^2. For perpendicular-contacting pillars (Supporting Information Figure S4c), the adhesion is equivalent to the sphere-on-the-flat configuration according to the JKR model[51]

$$F = \frac{3}{4}\pi W d \tag{8}$$

giving F = 2.6 N/cm^2 normalized by area. The actual adhesion should lie in-between the values given by Equations 7 and 8, depending on the horizontal skew angle θ_s between the contacting pillars (Supporting Information Figure S4d).[52] For the shear adhesion, the classical Kendall's peeling model[53] is adapted for cylindrical pillars[19](Supporting Information Figure S4e)

$$F = \sqrt{3}\left(\frac{\sqrt{(1-\upsilon^2)}\pi E d^4 W^2}{32}\right)^{1/3} \tag{9}$$

yielding F = 32.7 N/cm^2 normalized by area.

The measured adhesion values are in general much smaller than the calculated value for interweaved pillars but larger than the calculated value for indented pillars, as shown in Figure 7.

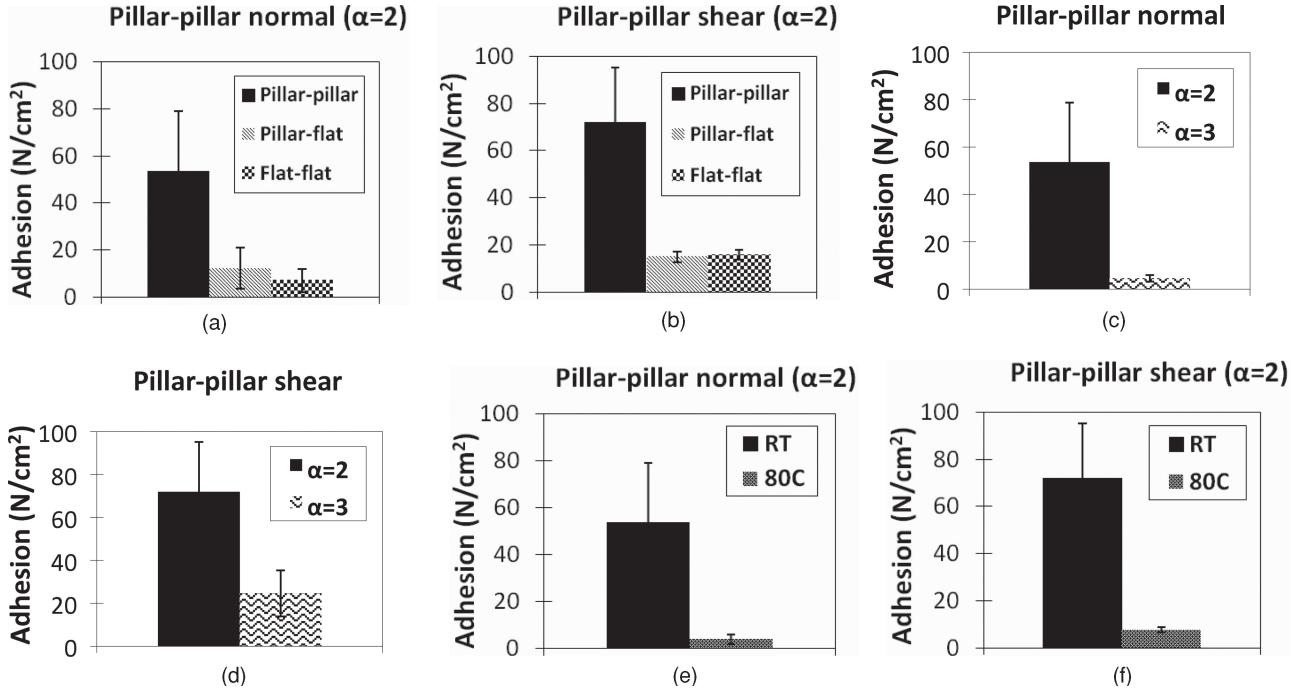

Figure 7. Measured pull-off force between two sets of hexagonal arrays of SMP pillars. a) The normal adhesion of $\alpha = 2$ (1 μm diameter, spacing 1 μm), aspect ratio 4 samples separated at room temperature in comparison to those from the pillar-to-flat and the flat-to-flat samples. b) The comparison for shear adhesion of the pillar-to-pillar, the pillar-to-flat and the flat-to-flat samples separated at room temperature. c) The pillar-to-pillar normal adhesion force of $\alpha = 2$ and $\alpha = 3$ (1 μm diameter, spacing 2 μm) samples separated at room temperature. d) The pillar-to-pillar shear adhesion force of $\alpha = 2$ and $\alpha = 3$ samples separated at room temperature. e) The normal adhesion force for $\alpha = 2$ samples separated at different temperatures. f) The shear adhesion for $\alpha = 2$ samples separated at different temperatures.

This trend can be explained by 1) the actual contact was a mixture of interweaving and indenting modes. The calculation of interweaved pillars provided an upper limit for the adhesion, whereas the adhesion for indented pillars offered the lower end. 2) The calculated values were obtained from the ideal scenario of either interweaved or indented pillar pairs. In reality, the contact was mostly likely non-ideal, where L_1, L_2, R, the contact geometry for the interweaved pillars, and the contact orientation for the indented pillars could be very different from pair to pair. Therefore, the actual normal adhesion for indented pillars should lie in between 2.6 to 18.3 N/cm^2. 3) The calculation assumed that the external load was evenly applied to all pillars. Experimentally, this could be hard to achieve, especially when the backing layer was rather thick (≈1–2 mm), which would promote stress concentration, thus, drastically lowering the measured adhesion values.[54] Supporting this was that the measured pillar-to-flat normal adhesion (12.3 ± 8.8 N/cm^2) which was about half the calculated value from Equation 7 (25.8 N/cm^2), while the shear adhesion (15.0 ± 2.3 N/cm^2) was ≈5 times smaller than the theoretical value from Equation 9 (82.3 N/cm^2). Here, the effective diameter d in Equations 7 and 9 was slightly modified for pillar-to-flat configuration, where d is expressed by

$$\frac{1}{d} = \frac{1}{d_1} + \frac{1}{d_2} \tag{10}$$

Here, d_1 and d_2 are the diameters of contacting surfaces, respectively. For pillar-to-pillar contact, $d_1 = d_2$ and $d = d_1/2 = d_2/2$. For pillar-to-flat configuration, assuming d_1 is the diameter of the pillar, then $d = d_1$ and the effective diameter is therefore doubled.

Nevertheless, the calculated adhesion qualitatively agreed with the experimental results, that is, the interweaved pillars had a higher adhesion over the indented pillars as evident by the superior adhesion strength (both normal and shear) of the pillar-to-pillar samples compared to that from the pillar-to-flat samples. Further supporting this was that the calculated values for indented pillars were always smaller than the experimentally measured pillar-to-pillar adhesion. In the pillar-to-flat samples, the only mode of contact is the buckled SMP pillars indented to the flat SMP film, making cylinder-to-flat contact, which is equivalent to the parallel cylinder-to-cylinder contact in the pillar-to-pillar case.

The relatively large standard deviation in adhesion measurement reflects the significant effect of small misalignment between the two pillar substrates and variation in the pillar-to-pillar contact from batch to batch. Specifically, the normal adhesion measurement itself is very sensitive to any misalignment because of the stress concentration,[55] resulting in larger errors in general than the shear adhesion values as evident from Figure 7. Measurement errors can be potentially minimized using a highly specialized instrument.[56,57]

We note that while the adhesion mechanism is completely different between gecko adhesion and Velcro adhesion, both are anisotropic, where attachment and detachment can be performed in a preferred direction. As we discussed above, the effective mode of the pillar-to-pillar contact at the interface is highly dependent on pillar geometry. Here, we quantify the adhesion anisotropy, ψ, as the ratio of shear to normal adhesion. When $\psi = 1$ the adhesion is isotropic. For $\alpha = 2$ pillars measured at room temperature, $\psi \approx 1.3$, close to isotropic regime. For $\alpha = 3$ pillars, the measured adhesion at room temperature is 4.5 ± 1.4 N/cm^2 in the normal and 24.6 ± 10.7 N/cm^2 in the shear separation, yielding a ψ value of ≈5.4. This strong anisotropy is similar to those reported in literature from random nanowires[28] and a periodic array of tilted nanopillar system.[26] However, the origin of the anisotropy is totally different in our system, where the pillars are buckled. In the case of nanowires and well-separated, tilted nanopillars, the enhancement of the shear adhesion was attributed to the increased contact area in the shear direction. In our system, the adhesion strength is highly dependent on pillar geometry, whether the pillars are in contact or not, degree of contact, and how they make contacts with each other. As discussed earlier, since the interweaved pillars offer much higher adhesion strength than the indented ones, we examined the change of anisotropy in the interweaved pillars by increasing the pillar spacing. In the interweaved pillar regime, the decrease in normal adhesion when increasing spacing is mainly owing to the smaller areal density of the pillars and the increase in effective lever arm for pillar deflection. When α increases from 2 to 3, the areal pillar density decreases by 56%, whereas the lateral average center to center distance (equals to $s + d$) between the interacting pillars rises by 50%. Therefore, if we recalculate the adhesion for $\alpha = 3$ sample, it is reasonable to assuming L_2 increases from 1 to 1.5 μm while all the other parameters are constant ($L_1 = 1$ μm, $R = 1$ μm and $\delta^p = \delta^s = 1.5$ μm). Thus, the normal force would decrease dramatically from 538 N/cm^2 for $\alpha = 2$ pillars to 141 N/cm^2 for $\alpha = 3$ pillars normalized by the nominal areal pillar density. In experiments, the normal adhesion force was found decreased by more than an order of magnitude, from 53.6 ± 25.1 N/cm^2 for $\alpha = 2$ pillars to 4.5 ± 1.4 N/cm^2 to $\alpha = 3$ pillars (Figure 7c). This suggests that when increasing the spacing, the possibility of pillars interweaving with each other decreases, thus, decreasing the adhesion strength. In fact, the separated interface of $\alpha = 3$ pillars often showed random collapsed pillars (Supporting Information Figure S6) rather than the Moiré patterns observed from $\alpha = 2$ pillars, suggesting less interweaved pillars during pillar-to-pillar contact. However, the lever arm in the shear direction should be nearly negligible since it is related mainly to L_1, which does not depend on the pillar spacing. Therefore, the decreases in shear adhesion with increasing pillar spacing should scale linearly with areal pillar density. Following this simple argument, the shear adhesion should decrease by 56% from $\alpha = 2$ to $\alpha = 3$ as 32 N/cm^2 experimentally, close to the measured one, 24.6 ± 10.7 N/cm^2 (Figure 7d). A more accurate estimation could be obtained by adding the torsional contribution of L_2 lever arm, which was neglected in Equation 6. For the indented pillars, the primary contribution is the decrease in effective contact area, which again would be decreased by 56%. Recall that for $\alpha = 2$ samples, the measured average pillar-to-flat normal and shear adhesion forces were 12.3 ±8.8 N/cm^2 and 15.0 ± 2.3 N/cm^2, respectively. For $\alpha = 3$ samples, if considering the sole contribution from the reduction in effective contact area, the pillar-to-flat adhesion should decrease to ≈5.5 N/cm^2 and ≈6.7 N/cm^2 in the normal and shear directions, respectively. Experimentally, the values were 4.1 ± 2.8 N/cm^2 and 10.3 ± 4.9 N/cm^2 in the normal and shear directions for $\alpha = 3$

samples, close to the predicted values. Clearly, the increase of adhesion anisotropy originated primarily from the interweaved pillars.

Another desirable characteristic of dry adhesives is the easy detachment on demand. As shown in Figure 7e,f, both the normal and shear adhesion dropped by an order of magnitude, from 53.6 ± 25.1 N/cm^2 to 3.6 ± 2.1 N/cm^2 and from 71.9 ± 23.2 N/cm^2 to 7.7 ± 1.0 N/cm^2, respectively, for α = 2 pillars when the samples were reheated at 80 °C. This can be attributed to the significant modulus drop above T_g, from 2.2 GPa at room temperature to 3.1 MPa at 80°C. According to Equations 5–9, except for JKR model, which predicts modulus independence, all the other models predict that the adhesion would decrease when modulus decrease. For the interweaved pillars, the separation force in either normal or shear direction scales linearly with the modulus, to 0.8 N/cm^2 for normal adhesion and to 13.2 N/cm^2 for shear adhesion. For the indented pillars, the decrease in adhesion depends on the contact geometry, which is down to 3.5 N/cm^2 based on cylindrical parallel-contact model (Equation 7) and to 3.6 N/cm^2 for indenting pillars by the peeling model for cylindrical pillars (Equation 9). Overall, the measured adhesion values, 3.6 N/cm^2 (normal) and 7.6 N/cm^2 (shear) at 80 °C, were within the range of the calculated values.

Lastly, we note that although the entropic energy stored in the deformed SMP pillars can be later released on demand upon reheating above T_g to trigger automatic debonding, the recovery of high-aspect-ratio SMP micropillars should be different from the recovery behavior of bulk SMP since the surface adhesion energy becomes significant for densely packed micropillars with feature size of 1 μm.[34] Buckled micropillars can be fully recovered only if the elastic restoring energy exceeds the adhesion energy between interweaved or indented pillars. While the low modulus at the rubbery state facilitates buckling and intimate interfacial contact between two opposing pillar surfaces for bonding, the subsequent cooling to room temperature results in high modulus at the glassy state, which favors high adhesion. When the interfacial width, thus effective contact area, between two deformed pillars is at maximum, the highest adhesion strength is expected. However, the maximum contact is unfavorable for the pillar recovery. In our experiments, the collapsed α = 2 pillars could not be recovered and α = 3 pillars were partially recovered after reheating. The observation is different from prior experiments involving SMPs in micropillars of much larger diameters (tens of μm) and not collapsed during bonding. Nevertheless, careful design of pillar geometry and fine-tuning of the T_g and elastic properties of the SMP will be investigated to find the balance of strong adhesion and recoverability of SMP pillars.

3. Conclusions

In summary, we designed a unique dry adhesive with strong adhesion based on buckling and interlocking between two sets of identical SMP pillar arrays. The SMP pillar arrays were engaged at 80 °C, above SMP T_g at a preload above the buckling threshold. The pillars were found interweaved and/or indented to each other from both experiments and FEA simulation. The strong bonding was achieved after cooling the interlocked sample to room temperature, upon which the SMP pillars became glassy. The deformed pillar-to-pillar contact led to very strong dry adhesion force at room temperature, ≈53.6 ± 2.1 N/cm^2 in the normal direction and ≈71.9 ± 23.2 N/cm^2 in the shear direction. These values are much larger than those from pillar-to-flat (12.3 ± 8.8 N/cm^2, normal and 15.0 ± 2.3 N/cm^2, shear) and flat-to-flat contact surfaces (7.1 ± 5.0 N/cm^2, normal and 15.8 ± 2.0 N/cm^2, shear). Our calculation using mechanical and contact mechanics models predicts that the pillar-to-pillar adhesion should lie between the scenario of interweaved and indented pillar-to-pillar contact, in good agreement with our experimental observations. For the interweaved pillars, FEA simulations and mechanical models further showed that the theoretical adhesion force could be comparable or surpassing the maximum tensile stress of the SMP, leading to pillar fracture. When increasing pillar spacing, we found that the adhesion strength was weakened while the adhesion anisotropy increased in both experiments and calculations, which could be attributed to the decreased number of the interweaved pillars. Moreover, we showed that the use of SMP could allow for easy separation simply by heating the interlocked pillars above T_g owing to the dramatic drop of elastic modulus. The interlocking adhesives reported here are, however, not reversible due to irreversible buckling of the small and tall pillars in a dense array. By varying the pillar geometry and size, it is possible to recover the deformed SMP pillars for reversible adhesion. Nevertheless, we believe the presented study of interlocking adhesion mechanisms based on buckling and tunable modulus, offer important insights of how to control the interfacial contact between pillars, which are critical to the design of strong dry adhesives in practice. In turn, it would open up a new path for creating structured surfaces for other applications, such as pressure sensors.[40]

4. Experimental Section

Materials and Fabrication: The poly(dimethylsiloxane) (PDMS) mold was prepared from the Si master, which was treated with (tridecafluoro-1,1,2,2-tetrahydrooctyl)trichlorosilane (Gelest Inc.) under vacuum. The degassed liquid PDMS prepolymer mixture (10:1 weight ratio, Sylgard 184, Dow Corning) was poured over the patterned Si wafer and cured at 65 °C for 4 h, after which the PDMS mold was carefully peeled off from the Si master.

The SMP precursors, bisphenol A diglycidyl ether (BADGE), poly(propylene glycol) bis(2-aminopropyl ether) (Jeffamine D-230) and decylamine (DA) were purchased from Sigma-Aldrich. The SMP adhesive was prepared following a similar formulation reported in literature.[58] Briefly, BADGE, Jeffamine D230 and DA were mixed at a molar ratio of 4:1:2. The mixture was then degassed by ultrasonication for 1 h, subsequently poured onto a PDMS mold, and thermally cured (100 °C for 1.5 h and 130 °C for 1 h). After cooling to room temperature, the cured SMP was carefully separated from the PDMS mold by peeling and the sample was cut into 1–2 cm^2. For bonding, two identical pillared SMP surfaces were pressed together at a preload of ≈24 N/cm^2 at 80 °C for 1 min, followed by cooling under the load.

Characterization: The T_g of the SMP was characterized using TA Q2000 differential scanning calorimeter (DSC) at a heating rate of 1 °C/min in nitrogen and TA Q800 dynamic mechanical analysis (DMA) at 1 Hz, 0.2% strain and a heating rate of 1 °C/min in nitrogen under "multifrequency, strain" mode.

The adhesion tests were carried out using Instron 4206 universal testing machine (UTM). The home-made sample holders for normal

and shear adhesion were attached to the load cell bearing a maximum load of 100 N (Supporting Information Figure S1). In a typical test, the crosshead moved at a speed of 0.02 in/min until the adhesion failure. The corresponding load-displacement data were collected using LabView (National Instruments). For adhesion test performed at 80 °C, the temperature was controlled using a hot plate or a heating gun equipped with temperature feedback control in the normal or shear adhesion tests, respectively. For all the temperature-dependent experiments, the samples were equilibrated at the designated temperature for at least 5 min.

The room temperature stress-strain curve of SMP was obtained using an Instron 4206. The load cell was 2.5 kN and the crosshead speed was 0.02 in/min. The stress-strain at 80 °C curve was recorded using TA Q800 DMA. The SMPs were equilibrated at 80 °C for 5 min, then stretched at a strain rate of 5%/min till reaching 5% strain. The Young's moduli of the SMP were determined from the linear portion of the corresponding stress-strain curves.

The adhesive surfaces separated by the UTM tests were examined using FEI Quanta FEG ESEM and FEI Strata DE235 scanning electron microscopes (SEM) at an accelerating voltage of 5 kV.

Finite Element Simulation: The single pillar pair and multiple pillar interaction models were meshed by 50424 and 4715 eight nodes hexahedral elements C3D8R per pillar, respectively. These models were calculated by Abaqus/Explicit. The simulation was performed using Simulia Abaqus 6.10-1. The bent pillar model was constructed using 120776 four nodes tetrahedral elements C3D4. This model was analyzed by Abaqus/Standard.

Supporting Information

Supporting Information is available from the Wiley Online Library or from the author.

Acknowledgements

This work was supported in part by the National Science Foundation (NSF) GOALI grant (# DMR-1105208) and Donors of the American Chemical Society Petroleum Research Fund (#50911-ND7). It reflects work performed by T.X. while at General Motors, prior to his employment at HRL Laboratories, LLC. The authors thank Professor Anand Jagota at Lehigh University for the helpful discussion of the adhesion mechanism. Kelvin Wong, Xiao Ciao, Issei Suzuki, Zheng Chen, and Hunter van Adelsberg are acknowledged for their assistance in sample fabrication and the preliminary work. Alex Radin is acknowledged for training the use of UTM and help on designing the adhesion measurement apparatus. Steve Szewczyk is acknowledged for the development of data acquisition software for UTM and training on the DSC. The Laboratory for Research on the Structure of Matter (LRSM), Penn NSF MRSEC (DMR-1120901), and Penn Regional Nanotechnology Facility (PRNF) are acknowledged for the access to the SEM. The authors also thank Penn State University's Nanofabrication Laboratory for fabrication of the photomask and silicon pillar masters. Equation 2 was corrected on July 12, 2013.

Received: January 6, 2013
Published online: March 6, 2013

[1] K. Autumn, M. Sitti, Y. C. A. Liang, A. M. Peattie, W. R. Hansen, S. Sponberg, T. W. Kenny, R. Fearing, J. N. Israelachvili, R. J. Full, *Proc. Natl. Acad. Sci. USA* **2002**, *99*, 12252.
[2] C. Creton, S. Gorb, *MRS Bull.* **2007**, *32*, 466.
[3] G. Huber, H. Mantz, R. Spolenak, K. Mecke, K. Jacobs, S. N. Gorb, E. Arzt, *Proc. Natl. Acad. Sci. USA* **2005**, *102*, 16293.
[4] K. Autumn, Y. A. Liang, S. T. Hsieh, W. Zesch, W. P. Chan, T. W. Kenny, R. Fearing, R. J. Full, *Nature* **2000**, *405*, 681.
[5] Y. Tian, N. Pesika, H. B. Zeng, K. Rosenberg, B. X. Zhao, P. McGuiggan, K. Autumn, J. Israelachvili, *Proc. Natl. Acad. Sci. USA* **2006**, *103*, 19320.
[6] B. X. Zhao, N. Pesika, H. B. Zeng, Z. S. Wei, Y. F. Chen, K. Autumn, K. Turner, J. Israelachvili, *J. Phys. Chem. B* **2009**, *113*, 3615.
[7] A. Ghatak, L. Mahadevan, J. Y. Chung, M. K. Chaudhury, V. Shenoy, *Proc. R. Soc. London Ser. A-Math. Phys. Eng. Sci.* **2004**, *460*, 2725.
[8] N. J. Glassmaker, A. Jagota, C. Y. Hui, J. Kim, *J. R. Soc. Interface* **2004**, *1*, 23.
[9] N. J. Glassmaker, A. Jagota, C. Y. Hui, W. L. Noderer, M. K. Chaudhury, *Proc. Natl. Acad. Sci. USA* **2007**, *104*, 10786.
[10] S. Kim, M. Sitti, *Appl. Phys. Lett.* **2006**, *89*, 3.
[11] A. del Campo, C. Greiner, E. Arzt, *Langmuir* **2007**, *23*, 10235.
[12] S. Reddy, E. Arzt, A. del Campo, *Adv. Mater.* **2007**, *19*, 3833.
[13] C. Greiner, A. del Campo, E. Arzt, *Langmuir* **2007**, *23*, 3495.
[14] M. K. Kwak, H. E. Jeong, T. I. Kim, H. Yoon, K. Y. Suh, *Soft Matter* **2010**, *6*, 1849.
[15] Y. Rahmawan, T. I. Kim, S. J. Kim, K. R. Lee, M. W. Moon, K. Y. Suh, *Soft Matter* **2012**, *8*, 1673.
[16] L. Ge, S. Sethi, L. Ci, P. M. Ajayan, A. Dhinojwala, *Proc. Natl. Acad. Sci. USA* **2007**, *104*, 10792.
[17] L. Qu, L. Dai, *Adv. Mater.* **2007**, *19*, 3844.
[18] L. T. Qu, L. M. Dai, M. Stone, Z. H. Xia, Z. L. Wang, *Science* **2008**, *322*, 238.
[19] J. Lee, C. Majidi, B. Schubert, R. S. Fearing, *J. R. Soc. Interface* **2008**, *5*, 835.
[20] J. H. Lee, R. S. Fearing, K. Komvopoulos, *Appl. Phys. Lett.* **2008**, *93*, 3.
[21] G. de Mestral, *U. S. Patent 2717437*, **1955**.
[22] G. de Mestral, *U. S. Patent 3,748,701*, **1973**.
[23] F. Allyn, B. Golden, *Why Didn't I Think of That: Bizarre Origins of Ingenious Inventions We Couldn't Live Without*, John Wiley & Sons, Inc., New York **1997**, p. 99.
[24] S. N. Gorb, R. G. Beutel, E. V. Gorb, Y. K. Jiao, V. Kastner, S. Niederegger, V. L. Popov, M. Scherge, U. Schwarz, W. Votsch, *Integr. Comp. Biol.* **2002**, *42*, 1127.
[25] S. N. Gorb, V. L. Popov, *Philos. Trans. R. Soc. Lond. Ser. A-Math. Phys. Eng. Sci.* **2002**, *360*, 211.
[26] C. Pang, T.-i. Kim, W. G. Bae, D. Kang, S. M. Kim, K.-Y. Suh, *Adv. Mater.* **2012**, *24*, 475.
[27] R. M. McMeeking, L. F. Ma, E. Arzt, *J. Appl. Mech.-Trans. ASME* **2009**, 76.
[28] H. Ko, J. Lee, B. E. Schubert, Y. L. Chueh, P. W. Leu, R. S. Fearing, A. Javey, *Nano Lett.* **2009**, *9*, 2054.
[29] H. Ko, Z. X. Zhang, Y. L. Chueh, J. C. Ho, J. Lee, R. S. Fearing, A. Javey, *Adv. Funct. Mater.* **2009**, *19*, 3098.
[30] H. Shahsavan, B. X. Zhao, *Langmuir* **2011**, *27*, 7732.
[31] S. Vajpayee, K. Khare, S. Yang, C. Y. Hui, A. Jagota, *Adv. Funct. Mater.* **2011**, *21*, 547.
[32] C. H. Pang, S. M. Kim, Y. Rahmawan, K. Y. Suh, *ACS Appl. Mater. Interfaces* **2012**, *4*, 4225.
[33] C. Pang, D. Kang, T.-i. Kim, K.-Y. Suh, *Langmuir* **2011**.
[34] Y. Zhang, C. W. Lo, J. A. Taylor, S. Yang, *Langmuir* **2006**, *22*, 8595.
[35] D. Chandra, S. Yang, *Acc. Chem. Res.* **2010**, *43*, 1080.
[36] R. Wang, T. Xie, *Chem. Commun.* **2009**, *46*, 1341.
[37] R. Wang, T. Xie, *Langmuir* **2010**, *26*, 2999.
[38] T. Xie, X. C. Xiao, *Chem. Mater.* **2008**, *20*, 2866.
[39] S. Kim, M. Sitti, T. Xie, X. C. Xia, *Soft Matter* **2009**, *5*, 3689.
[40] C. Pang, G.-Y. Lee, T.-i. Kim, S. M. Kim, H. N. Kim, S.-H. Ahn, K.-Y. Suh, *Nat. Mater.* **2012**, *11*, 795.
[41] A. Lendlein, S. Kelch, *Angew. Chem. Int. Ed.* **2002**, *41*, 2034.
[42] P. T. Mather, X. F. Luo, I. A. Rousseau, *Ann. Rev. Mater. Res.* **2009**, *39*, 445.

[43] T. Xie, *Polymer* **2011**, *52*, 4985.
[44] C. Y. Hui, A. Jagota, Y. Y. Lin, E. J. Kramer, *Langmuir* **2002**, *18*, 1394.
[45] S. Timoshenko, *Theory of Elastic Stability*, McGraw-Hill, New York **1961**.
[46] I. Amidror, *The Theory of the Moiré Phenomenon*, Springer London, London **2009**.
[47] S. H. Kang, N. Wu, A. Grinthal, J. Aizenberg, *Phys. Rev. Lett.* **2011**, *107*, 177802.
[48] C. T. F. Ross, *Mechanics of Solids*, Prentice Hall, London, New York **1996**.
[49] C. S. Davis, A. J. Crosby, *Soft Matter* **2011**, *7*, 5373.
[50] J. Li, Y. An, R. Huang, H. Jiang, T. Xie, *ACS Appl. Mater. Interfaces* **2012**, *4*, 598.
[51] K. L. Johnson, *Contact Mechanics*, Cambridge University Press, Cambridge Cambridgeshire; New York **1985**.
[52] B. Sumer, C. D. Onal, B. Aksak, M. Sitti, *J. Appl. Phys.* **2010**, 107.
[53] K. Kendall, *J. Phys. D-Appl. Phys.* **1975**, *8*, 1449.
[54] S. Kim, M. Sitti, C. Y. Hui, R. Long, A. Jagota, *Appl. Phys. Lett.* **2007**, 91.
[55] M. Kamperman, E. Kroner, A. del Campo, R. M. McMeeking, E. Arzt, *Adv. Eng. Mater.* **2010**, *12*, 335.
[56] E. Kroner, J. Blau, E. Arzt, *Rev. Sci. Instrum.* **2012**, 83.
[57] E. Kroner, D. R. Paretkar, R. M. McMeeking, E. Arzt, *J. Adhes.* **2011**, *87*, 447.
[58] T. Xie, I. A. Rousseau, *Polymer* **2009**, *50*, 1852.